pH-dependent Polyelectrolyte Bridging of Charged Nanoparticles

Morten Stornes, Binamra Shrestha, and Rita S. Dias*

Department of Physics, NTNU - Norwegian University of Science and Technology, NO-7491 Trondheim, Norway

E-mail: rita.dias@ntnu.no

Abstract

Systems comprised of polyelectrolytes and charged nanoparticles are of great technological interest, being common components in formulations among other uses. The colloidal stability of formulations is an important issue, and thus a large effort has been made to study the interactions of individual components in these systems. Here, the complexation and adsorption of an annealed (pH-dependent) polyelectrolyte to two spherical nanoparticles has been studied using coarse-grained Monte Carlo simulations. This has been done mainly by varying the solution pH and separation distance (concentration) between the nanoparticles. The polyelectrolyte charge distribution is seen to vary with nanoparticle separation distance and its ability to bridge both nanoparticles changes with pH. The flexible polyelectrolyte creates compact, multi-link bridges at short nanoparticle separation distances, and evolves to a stretched single-link bridge at longer distances, where a larger fraction of the polyelectrolyte wraps around the nanoparticles. The annealed polyelectrolyte is also compared with a quenched polyelectrolyte of similar fixed fractional charge. Here, it is found a difference in adsorption ability at low pH/ionization due to the ability of the annealed polyelectrolytes to concentrate charges in the vicinity of the nanoparticle. At intermediate polyelectrolyte charge fractions and with increasing nanoparticle separation distances, the annealed system is able to link nanoparticles at larger distances as compared to the quenched, in good agreement with experimental observations. The results in this work contribute to the understanding of the effect of annealed polyelectrolytes and pH variations in the phase behaviour of polyelectrolyte-nanoparticle systems, potentially aiding in the design and optimization of pH-responsive systems.

Introduction

Polyelectrolytes (PEs), both natural occuring and synthetic, are used in multiple industrial applications, for example as rheological modifiers, flocculants or solution stabilizers. Applications include removal of organic waste from wastewater and stabilizing formulations used in food, paint and cosmetic applications. PEs are also ubiquitous in nature, since most biopolymers, such as proteins, polysaccharides and nucleic acids, possess charged groups.

PEs typically interact with other macromolecules, both neutral and charged, which could be other PEs, cell membranes, micelles, or synthetic nanoparticles (NPs). Furthermore, the interaction between e.g. NPs can be mediated by polymers and PEs. Neutral, nonadsorbing polymers may induce depletion attraction, while polymers that adsorb or are grafted onto NPs can cause steric repulsion and act as a stabilizer in NP solutions.[1–6] PEs, which are electrostatically charged, will also influence interactions between charged NPs. This can be done e.g. through neutralization of the surfaces, causing attractive van der Waals interactions to dominate the interactions, or charge reversal of a PE-NP complex, creating repulsive interactions. In some situations, the PE will also adsorb to two or more surfaces, giving rise to attractive bridging forces between particles. This has been explored for self-assembly of macromolecular complexes.[7] The characteristics of such systems may be adjusted by changing properties of the adsorbing surface, such as charge density or geometry, the temperature or the ionic strength of the solution, or properties of the PE, such as chain stiffness, charge density, chain length, etc.

DLVO theory, which describes a mean-field interaction between charged particles in liquids, is suitable for describing many of these systems where van der Waals and electric double layer interactions dominate, at least at interaction distances above a few nm. Other theoretical methods have been developed to study more complicated systems, such as those where the PE can sufficiently screen the interaction, the PE density influences adsorption and aggregation, ion correlations are prevalent or where the surfaces are close enough for PE bridging. These methods include approaches based on self-consistent field theories, variational methods and density functional theory[8–15] along with numerical modelling.[16–20] Experimentally, these systems have been studied using a variety of methods, including phase diagram determination, surface force apparatus, atomic force microscopy and optical tweezers for force measurements and scattering techniques for size and structure determination.[6,21–31]

Due to the rich variety of PE-NP systems, there are still unexplored areas. Much of the non-experimental work tends to focus on quenched, or strong, PEs. These have a fixed homogenous charge distribution independent of solution pH. This is as opposed to annealed PEs, where monomers contain weak, or titratable, acidic/basic groups that can deprotonate/protonate, de-

pending on the pH of the solution. This can lead to phenomena such as charge regulation.

While the force acting between spherical particles can be related to that of flat surfaces through the Derjaguin approximation, any conformational properties of PE-NP complexes are potentially lost if only flat surfaces are considered. These could in turn influence the interaction behaviour through PE mixing or ion correlations. There has also been much work done on systems consisting of a single NP and annealed PE,[32–36] but to understand the impact of annealed charges on NP solution stability, for example, one needs at least two NPs. Some work has been done involving multiple free NPs adsorbing on a single long, annealed PE,[20] with a special focus on the PE stiffness. In this work, we consider a system consisting of a single, annealed PE and two oppositely charged, spherical NPs. Utilizing a coarse-grained particle model, we have used Monte Carlo simulations to investigate the adsorption of the PE onto the NPs, the PE bridge formation between them and PE conformational properties. This is done for different pH and separation distances between the NPs, which here roughly mimics NP concentration.

Computational Details

We have used a simple coarse-grained model of nanoparticles and a polymer in a salt-free solution. The system consists of two nanoparticles and a polymer inside a hard cylindrical boundary of radius 200 Å and length 600 Å with the radial direction in the yz-plane. The boundary size is large enough to avoid constraints due to high particle density. The nanoparticles are hard spheres with a radius of 20 Å, a fixed point-charge of $60e$ each, and are fixed in place with a separation distance d, defined as the closest distance between the NP surfaces. The polymer is a flexible, linear chain of 60 monomers, placed at a random location in the simulation cell. Each PE monomer has a radius of 2 Å and a charge of 0 or -1e for the annealed PE, while the monomers of the quenched PE have fixed monomer charges at $z = -\alpha$ with $\alpha \in [0, 1]$ being the fractional ionization of the PE. Each monomer has a corresponding counterion and each NP has 60 counterions, to keep the system charge neutral. All counterions are modelled as hard spheres of radius 2 Å. The system is solved in the canonical ensemble.

4

Monomers can change between a charged and neutral state, and a corresponding counterion charge is also flipped between neutral/charged at the same time. The solvent enters the model through the relative permittivity, and is not explicitly modelled.

The Metropolis Monte Carlo scheme is employed, with the potential energy of the system given by

$$U = U_{non-bond} + U_{bond} \tag{1}$$

where $U_{non-bond}$ combines the electrostatic potential with the hard-sphere repulsion so that

$$U_{non-bond} = \sum_{i<j} u_{ij}(r_{ij}), \tag{2}$$

for particles i and j at a separation r_{ij}. For particles with charge ze and radius R,

$$u_{ij} = \begin{cases} \infty, & r_{ij} < R_i + R_j \\ \frac{z_i z_j e^2}{4\pi\varepsilon_0\varepsilon_r r_{ij}}, & r_{ij} \geq R_i + R_j \end{cases}, \tag{3}$$

where ε_0 and ε_r denote the vacuum and relative permittivity. The potential energy of the bond is given by

$$U_{bond} = \frac{k_{bond}}{2} \sum_i^{N_{bond}} (r_{i,bond} - r_0)^2, \tag{4}$$

where k_{bond} is the force constant, r_0 the equilibrium separation and $r_{i,bond}$ the bond length.

As monomers protonate/deprotonate, there is a change in the potential energy, given by

$$\Delta U_{prot} = k_B T \ln 10 (\text{pH} - \text{p}K_a)\Delta z, \tag{5}$$

where k_B and T are the Boltzmann constant and temperature and $\text{p}K_a = -\log K_a$, where K_a is the acid dissociation constant of the polymer.[37] By using a mean field approximation, where we assume that all titration sites have the same apparent $\text{p}K_a$, the average PE fractional ionization α is related to the $\text{p}K_a$ by[38]

$$\text{p}K_a = \text{pH} - \log\frac{\alpha}{1-\alpha}. \tag{6}$$

As $\alpha \to 0$, pK_a goes toward that of a monoprotic acid, pK_0. Assuming that all monomers have a dissociation constant of K_0, the difference in potential energy which determines the probability of flipping a charge is given by

$$\Delta U = \Delta U_{el} + k_B T \ln 10 (\text{pH} - pK_0) \Delta z. \qquad (7)$$

Here, $\text{pH} - pK_0$ is given as input to the program and the ionization of the annealed PE is calculated according to $\alpha = \sum_{i=1}^{N_{mon}} |z_i| / N_{mon}$ where N_{mon} is the number of monomers in the PE chain.

Fixed parameter values used in this work are $T = 298$ K, $\varepsilon_r = 78.4$, $k_{bond} = 0.4$ Nm^{-1} and $r_0 = 5$ Å.

Monomers are considered adsorbed if they are within the adsorption threshold of 3 times the PE monomer radius, 6 Å, which is within the Bjerrum length.

All simulations were done using the MOLSIM package.[39] For each step in the simulation, each particle is selected once and a Metropolis move is attempted. Moves include translation of the particle (monomers and counterions), translation or pivoting of the chain (monomers only), and charge flipping. For the annealed monomers, this occurs with a probability of 1/3 for particle translation and charge flipping, and 1/6 for chain translation and pivoting. The results of multiple steps are averaged in a macrostep, and the results given are the grand averages over multiple macrosteps. As the system configuration is not reset between different macrosteps, the resulting equilibrium state of the system could be dependent on the initial condition. This is particularly the case at large NP-NP separation distances, the electrostatic influence of one NP at the surface of the other could be small enough to give rise to an asymmetric system configuration. Due to the simple symmetry of the NPs, any results considering the distribution of particles along the system can in principle be mirrored to display the resulting ensemble average.

Results and discussion

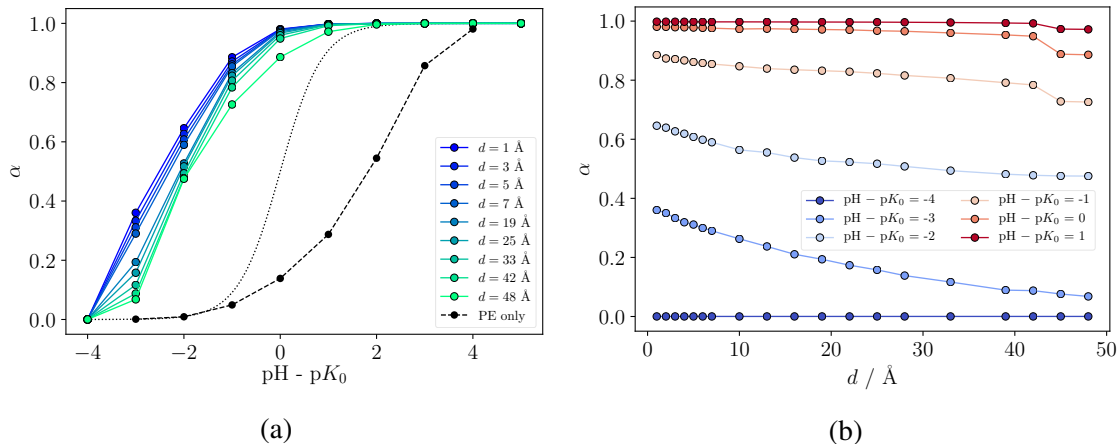## Titration behaviour and charge distribution

Figure 1: (a) Titration curves for different separation distances d. Dotted curve show the ionization of a solution consisting only of PE monomers. (b) Average monomer charge as a function of separation distance d for different $\mathrm{pH} - \mathrm{p}K_0$. The discontinous drop in charge at the longest distances is due to the polymer adsorbing primarily to a single NP.

Starting off, we consider the titration behaviour of the PE in absence of NPs by assessing the average fractional charge, α, of the PE as a function of pH. As observed previously,[32,40,41] larger pH values are needed for the PE to reach the same ionization degree as the corresponding unbound monomer (dotted vs. dashed line in Fig. 1a), and the effect increases with chain length, due to electrostatic monomer-monomer repulsion. In the presence of oppositely charged macroions, PEs ionize at an increased rate and, provided a sufficiently strong electrostatic field, will ionize faster than a (dilute) solution consisting of only single PE monomers. As can be seen in the titration curves in Fig. 1a, fractional ionization also depends on the distance between the NPs. By fixing the NPs at a distance d, we observe an increased PE ionization for shorter d (darker blue lines); as it will be shown below, the PE is found between the two NPs and the close proximity promotes monomer ionization. As the distance increases, the ionization decreases slightly. A larger difference arises when d is long enough that the PE primarily adsorbs on a single NP, as can be seen by comparing $d = 42$ Å and 48 Å between $\mathrm{pH} - \mathrm{p}K_0$ of -2 – 1.

Fig. 1b shows the fractional PE charge as a function of the NP separation distance for increasing $pH-pK_0$. As would be expected, α does not vary with the NP distance for the extreme values of $pH-pK_0$, where the PE is either fully charged or neutral. When considering intermediate values, the drop in the average monomer charge with increasing NP distance tends to be larger for lower pH values. This can be attributed to the decreased probability of the PE to bridge the NPs as is discussed further down.
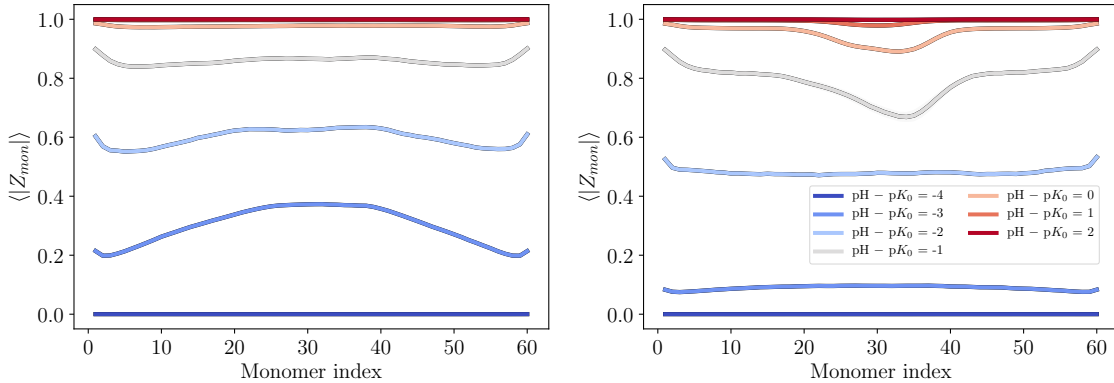

Figure 2: Average monomer charge for $d = 6$ (left) and $d = 39$ (right) Å.

We also consider the charge of the individual PE monomers for increasing $pH-pK_0$, with varying NP separation distance. Similar monomer charge profiles have been done for free[32,40] and adsorbed[41] linear chains, as well as star polymers[42] and gels.[43] Fig. 2 shows the average monomer charge, $|Z_{mon}|$, for each monomer along the PE chain for two different separation distances, 6 and 39 Å. In general, $|Z_{mon}|$ increases with increasing values of $pH-pK_0$. For shorter d (left-hand panel) the central monomers are most likely to be charged, as these tend to cluster between the NPs, while the tails keep some of their conformational entropy by not adsorbing strongly to the NPs. This leads to a lower charge toward the end of the chains. The end monomers have a slightly larger probability to be ionized, due to reduced intramolecular electrostatic repulsion, and the charge profile is similar to those of a PE adsorbed on a single NP, shown in other works.[41]

At longer distances (right-hand panel), the central part of the PE has a decreased ionization probability at higher pH, as seen by the dip around monomer 30. At these distances, given a sufficiently high α, the PE forms a single bridge between the NPs, and that leads to the more

charged ends in contact with the NPs and less charged centre of the chain, which is less often in contact with the NPs, leading to the clear dip in the center of the chain. This can also be seen in the bottom left panel of Fig. 3. For small $\text{pH}-\text{p}K_0$ ($\leq$ -2), the PE rarely bridges the NPs, giving charge profiles similar to those for free PE or PE adsorbed to a single NP. End monomers have a further increase in charge probability, again due to intrachain repulsion.
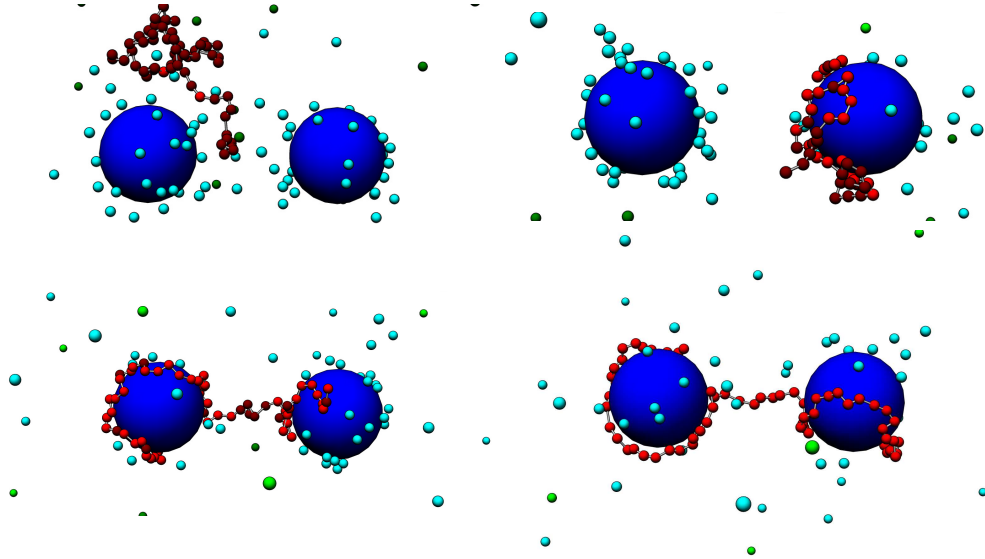

Figure 3: Example of system at $d = 39$ Å for increasing pH with $\text{pH}-\text{p}K_0$ = -3 (top left), -2 (top right), -1 (bottom left) and 4 (bottom right). Dark red monomers are neutral, bright red are charged. Blue and green particles are the respective counterions of the NPs and PE monomers.

Particle density distribution

Fig. 4 shows the density distribution of the PE (top) and the NP counterions (bottom) along the lateral direction of the cylindrical boundary, for different $\text{pH}-\text{p}K_0$ values. PE counterions are not included, as they tend to have a fairly uniform distribution throughout the system, with reduced density around the NPs. The systems shown here are for three different d, where the PE bridges the NPs at short and long distances ($d = 7$ and 39 Å), and when there is no bridging ($d = 48$ Å). For the systems where the PE does not bridge, the density distribution is asymmetric at $\text{pH}-\text{p}K_0 \geq$ -2, as the PE stays adsorbed on the first NP it adsorbs to. This is dependent on the initial conditions of the system, and the density distributions are expected to be symmetric in an ensemble average.
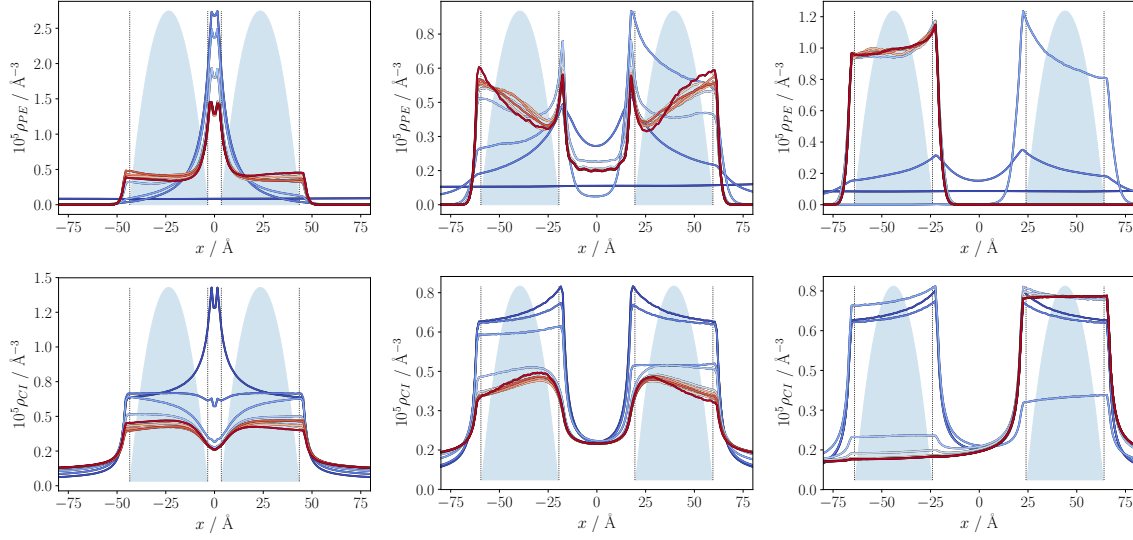
Figure 4: Density distributions for PE (top) and counterions of the NP (bottom) for $pH-pK_0$ ranging from -4 (dark blue) to 5 (dark red). Dotted vertical lines show the edges (in axial direction) of the NPs, and the shaded areas show the (normalized) cross-sectional area covered by NPs. NP-NP separation distances are $d = 7$ Å (left), 39 Å (middle), and 48 Å (right).

At short separation distances, as seen here for $d = 7$ Å, the PE is weakly charged at low pH and concentrates mainly in the space between the NPs (which we here define as inner) for $pH-pK_0$ = -3 and higher (the PE is neutral at $pH-pK_0$ = -4 and can be anywhere in the system). With increased pH (dark blue to dark red), the monomer density in the center is reduced, as the PE charge increases and the chain starts wrapping more around the NPs. For the fully charged PE, the monomer density is still largest in the center, with the PE forming multiple links between the NPs. With increasing d, the central monomer density is reduced, as the system goes to a single-link configuration. Here, the monomer density is largest close to the inner surface of the NPs at low pH, as seen for $d = 39$ Å. In this particular system, the PE begins adsorbing to both NPs at $pH-pK_0$ = -2, whereas at $pH-pK_0$ = -3, it is insufficiently charged, and will at times not be adsorbed to either NP, but instead residing between the NPs, and potentially outside them as well. This gives rise to the increased monomer density around $x = 0$ for $pH-pK_0$ = -3 (dark blue curve). At $pH-pK_0$ = -2, the PE density distribution is asymmetric, as the PE adsorbs to the NP surfaces, but is not capable of forming a stable bridge (discussed further down). The asymmetry in the distribution is expected to disappear with increased run time as the PE switches between the NPs, but the figure was kept asymmetric

10

to highlight the single NP adsorption behaviour. The PE continues to wrap around the NPs at larger pH values, although the increased distance between the NPs means the PE will be too short to wrap around the outer surface and come back to the inner surface, as illustrated in the bottom panels of Fig. 3. This, combined with the reduced electrostatic attraction from the opposing NP with increasing distance, gives a larger monomer density on the outer half of the NPs. When the distance between the NPs is sufficiently large, here shown for $d = 48$ Å, the PE only adsorbs to a single NP. At $pH - pK_0 = -3$, the PE adsorbs occasionally to one of the NPs, while also residing in the inner space between them, as can be seen by the profile similar to the one for $d = 39$ Å (note the different scale). From $pH - pK_0 = -2$ and higher, the PE has a large enough charge to strongly adsorb to one NP only. This is clearly featured in Fig. 4 (top right panel) showing examples where the PE adsorbs to the NP on the right or the left-hand side. The asymmetry in the adsorption profile around the NP, is due to a net electrostatic attraction from the opposing NP, which is not fully neutralized by adsorbed counterions. The monomer distribution between the NPs as seen here for $d = 7$ and 39 Å, has a similar shape to what has been previously shown for quenched PEs bridging flat[12,18,44] and spherical[45] surfaces, with a larger monomer density closer to the surface than in the center between the surfaces.

The NP counterions tend to have a larger density close to the inner surface of the NPs, particularly at low pH where the PE is not fully charged. For the shortest separation distances, the counterions have a large density between the NPs when the PE is neutral (darkest blue curve), but they are pushed away as the PE occupies the space with increasing pH. Still, a number of counterions are adsorbed to the NPs. We recall that the fully charged PE only neutralizes one NP. At larger distances ($d = 39$ Å), the counterions still maintain a larger density around the inner half of the NPs. At low pH, this is mainly due to the electrostatic attraction from the opposing NP. With increasing pH, the counterion density around the NPs decreases, as the number of adsorbed PE monomers and PE charge density increases. Again, the counterion density becomes larger on the inner half of the NP surface, now due to the lower occupancy of the PE in that region. Considering now the longest NP-NP separation distance, the profiles at low pH are similar to those at NP distances sufficiently long for a single PE link to be formed (here shown for $d = 39$ Å). At the highest pH, when the PE is fully charged,

the profiles are asymmetric with the counterions only adsorbing to the PE-free NP. The NP counterion density profile around the NP which the PE is not adsorbed to is flat, as the PE fully neutralizes the NP, causing zero net electrostatic attraction to the single NP-PE complex.
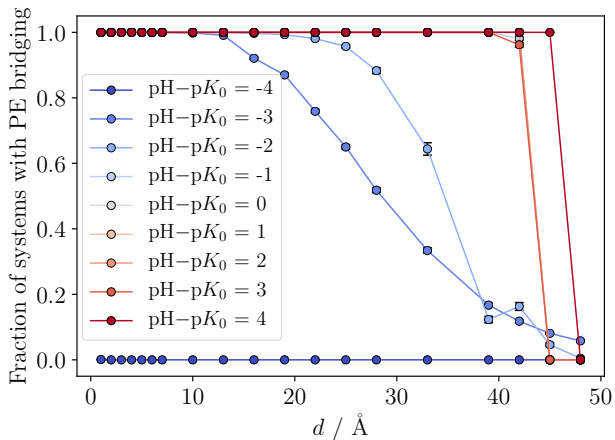

Figure 5: Fraction of sampled configurations where the PE is considered adsorbed to both NPs as function of distance, for selected pH. Error bars show one standard deviation of the sample mean.

As mentioned, the PE adsorbs to both NPs unless the distance between them becomes too large. As the PE stretches out and becomes stiffer as its charge increases, the NP-NP separation distance at which the PE is capable of forming a bridge, increases with increasing pH (Fig. 5). For high pH values, the PE adsorbs to both NPs up to separation distances of $d \approx 42 - 45$ Å, a distance approximately 2/3 of the gyration radius for a free, fully charged PE. The transition from bridging to single NP adsorption also explains the drop in the average PE fractional charge for the highest values of $pH-pK_0$ at these distances, seen in Fig. 1b.

It can be seen in Fig. 5 that the maximum distance for stable bridge formation is reduced at lower $pH-pK_0$. At $pH-pK_0 = 4$, the distance for bridging is at its largest, although the difference in PE charge compared to lower $pH-pK_0$ is small. In the range $pH-pK_0 = 3$ to -1, the difference is small, even though the fractional ionization of the chain reduces with pH. While the system with $pH-pK_0 = -1$ or 0 will on average have fewer charged monomers than at $pH-pK_0 = 2$ and above, these will mainly be located closer to the center of the chain, which resides between the NPs, while the outer parts of the PE which are located closer to the NPs, are sufficiently charged to stay adsorbed (see Fig. 2). Further reducing the pH, the probability of forming bridges at large NP-NP separations drop, as seen for $pH-pK_0 =$

-2 and even more for $\text{pH}-\text{p}K_0 = -3$. The kink seen here for $\text{pH}-\text{p}K_0 = -2$ at $d = 42$ Å, arises due to a particularly stable bridge forming during the run, which bridges the NPs over multiple successive macrosteps, which increases the contribution to the results. It is expected that this particular kink, which is not observed in similar systems presented in the supplementary materials, would disappear with increased run time. At $\text{pH}-\text{p}K_0 = -3$, the probability of forming bridges does not drop to zero even at the longest studied distances. This can be attributed to the low charge of the PE, which makes the chain more mobile as it does not strongly associate with the NPs, while not being as free as the completely neutral PE at $\text{pH}-\text{p}K_0 = -4$.

It should be mentioned that the chosen adsorption threshold could potentially influence the results in Fig. 5. In the case of PE monomers adsorbing and remaining close to the surface of both NPs, the adsorption threshold should not influence the results much. If, however, the PE is freely floating between the NPs, a larger adsorption threshold will likely increase the bridging probability shown in Fig. 5. Based on the monomer density distributions in Fig. 4, we see that this is not the case here for the annealed PE, which tends to adsorb to the surface. For a quenched PE with low α (discussed later), this might be the case as these systems tend to have the PE occupying the space between the NPs in a more condensed conformation.

These results suggest that NP aggregation can be controlled by variations in pH. Provided that the annealed PEs are added at relatively low or high concentrations, that is, inducing the formation of under- or overcharged complexes, and the NP concentration is sufficiently low so the average NP separation is sufficiently large, the formation of charged individual NP-PE complexes or that of larger complexes where the PEs bridge two or more NPs can be tuned by changing the pH.

The importance of pH variation in formulation stability was demonstrated experimentally in the preparation of hybrid hydrogels composed of nanoparticles with pH-sensitive surface groups and oppositely charged annealed PEs.[46] If the components were added at a pH where both were charged, a white precipitate would be formed, indicating the formation of neutral complexes. However, addition of neutral NPs to the polymer solution and a slow decrease of the pH leads to the formation of hydrogel with the NPs serving as cross-links, that is, the PE

did presumably bridge different NPs. While the authors state that slow pH variation induces hydrogen bond formation between the components leading to gel formation, our results suggest that the bridging and aggregation could instead be due to the electrostatic interactions between the PEs and NPs, as decreasing the pH from a high value would slowly increase the NP charge, while the PE will remain highly charged. This would imply that the PE is stretched out and capable of bridging NPs at larger distances, while the small NP charge would not necessarily cause the PE to adsorb fully to a single NP due to overcharging of the complex.

We have seen previously[41] that at low pH values, when the PEs are weakly charged, the adsorption on a NP is different for the pH-dependent annealed PEs and the quenched PEs, where each monomer has a fixed charge $z = -\alpha$. Here we use the NP-PE radial distribution functions (Fig. 6) to assess the difference in adsorption between annealed and quenched PEs at two different pH values and three separation distances, d. For pH$-$pK_0 = -3 (note the difference in α for the three separation distances), we can see a clear shift of the quenched PE profile to the right, indicating a weaker adsorption compared to the annealed PE. The difference between the quenched and annealed PEs disappears at larger α, as shown here for $\alpha \geq 0.48$ where the difference is miniscule.

The difference in adsorption profile can be explained by the difference in the local charge density due to mobile charges along the chain. The annealed PE, which has a few charged monomers ($z = -1$), has a strong local charge along a few points in the chain, while the rest is neutral. This promotes a strong adsorption to the NP at a few charged points situated closely together on the PE due to the charge mobility. The quenched PE, on the other hand, has an even charge distribution along the entire chain. Each monomer then interacts weakly with the NP, while also slightly repelling neighbouring monomers. This leads to larger segments of the quenched chain being attracted to both NPs. One could imagine a heterogenous quenched polymer with an even distribution of charged and neutral monomers along the chain, which could potentially have an adsorption profile more similar to that of the annealed PE. Based on our previous work[41] where the heterogenous and homogenous quenched PEs showed similar adsorption behaviour on a single NP, while differing from the annealed PE, we do not expect this to be the case, as charge mobility seems to be the main cause of the difference in

14

adsorption.

Considering the density distributions in Fig. 6 (bottom panels), specifically the annealed PE at pH$-$pK_0 = -3 (blue lines) and the corresponding quenched PE (dashed, blue lines), it is clear that the monomers of the quenched PE are largely situated in the inner space between the NPs. This is as opposed to that of the annealed PE, which tends to have a larger density close to the surface of the NPs where the ionized monomers are likely to be located, as discussed above. This behaviour is kept for a wide range of d values. At the largest distances, the annealed PE tends to be less associated when compared to the quenched PE. This can be seen in snapshots (not shown) and is also indicated by the increased monomer density on the outer side of the NPs, as seen for $d = 39$ Å. α for the annealed PE denotes the average charge, and at times the PE will be neutral and free, while the quenched PE tends to be located around the NPs due to the electrostatic attraction. While interesting, it is presently unclear to us if and how this difference in adsorption behaviour will be reflected on the macroscopic behaviour and colloidal stability of these systems. This would surely be different in other systems, e.g. with strong van der Waals forces, which would allow for a stronger adsorption of the annealed PE, again leading to a larger charge fraction due to the increased interaction with the NP. At pH$-$pK_0 = -2, where the PE charge is about half of the fully charged case, the density distribution is very similar for annealed and quenched PEs for d less than approximately 35 Å, as can be seen in Fig. S1. As d increases above this, the annealed PEs have a slightly higher probability of forming bridges compared to the quenched, which prefers to adsorb to a single NP. Indications of this can be seen here in the monomer density distribution at $d = 39$ Å (Fig. 5), while the bridging probability for the quenched and annealed systems at different distances is shown in the supplementary materials (Fig. S2).

We see here that the charge mobility of the annealed PE can potentially enhance NP aggregation and formation of large NP-PE complexes compared to quenched systems. This is in good agreement both with simulations performed with multiple free NPs and a long PE,[20] and with experimental phase diagram determinations where PE-NP complex salts prepared with quenched and annealed PEs were compared. In the simulation study, the adsorption of NPs on the PE is shown to differ between annealed and quenched for $\alpha < 0.40$. In the experimental

systems, the quenched PEs were shown to lose long-range order at higher PE charge fractions than salts with a corresponding annealed PE.[31] In other words, the annealed PE bridges the surfactant micelles (which can roughly be treated as a charged NP) more efficiently for a wider range of PE charge fraction. Annealed PEs have also been shown experimentally to enhance the formation of macroscopic complexes composed of PEs and surfactant micelles or proteins.[47,48]
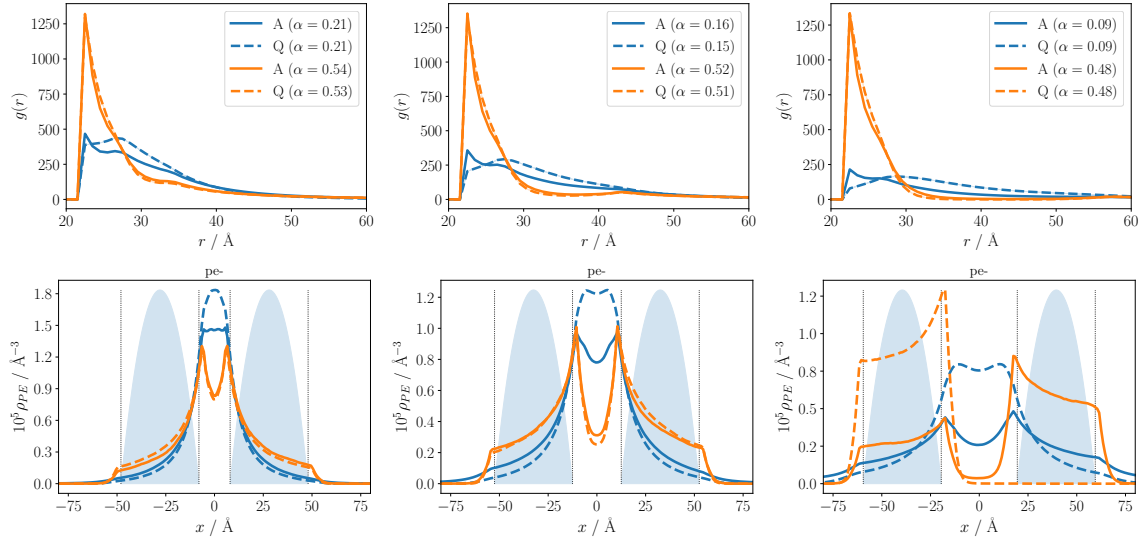

Figure 6: Radial distribution functions (top) and density distributions (bottom) for annealed (full lines) and quenched (dashed lines) PEs at separation distances $d = 16$ Å (left), 25 Å (middle) and 39 Å (right). The systems with annealed PEs are for pH$-$pK_0 = -3 (lowest α, blue lines) and -2 (highest α, orange lines). Note similar profile for pH$-$pK_0 = -2, as the average PE charge is large enough for the quenched PE to adsorb strongly.

Conformational behaviour

The conformational behaviour of the PE has been evaluated using the radius of gyration, R_g, and the end-to-end radius, R_{ee}, as a function of d with fully charged PE (Fig. 7) and as a function of pH with fixed NP-NP separation (Fig. 8). Starting with Fig. 7, it can be seen that with increasing d, the PE chain becomes stretched out, which results in an increase in both the radius of gyration and end-to-end radius. The R_{ee} distribution evolves from bimodal to unimodal with increasing d, as the system goes from having multiple links between the NPs, where both ends of the chain can be located on the same NP, to a single link configuration.
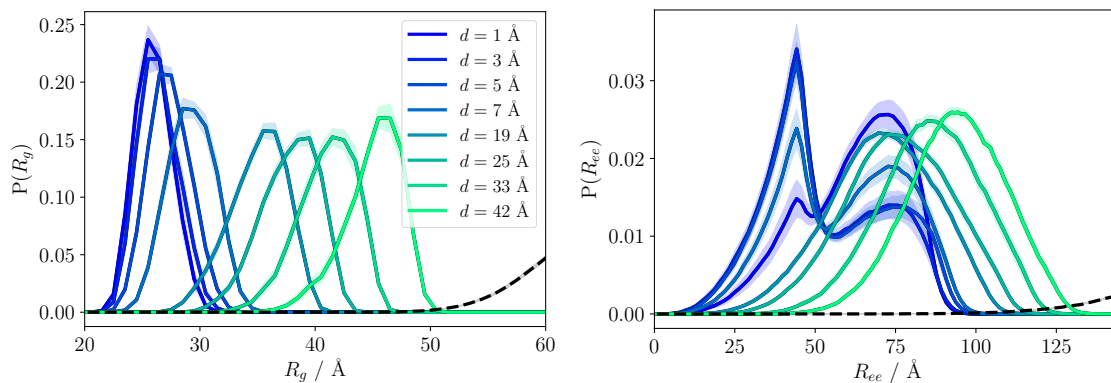
16

Figure 7: Radius of gyration (left) and end-to-end radius (right) for different d at $pH-pK_0 = 4$, i.e. fully charged PE. Dashed line shows system with PE only, shaded area shows one standard deviation of the sampled mean.
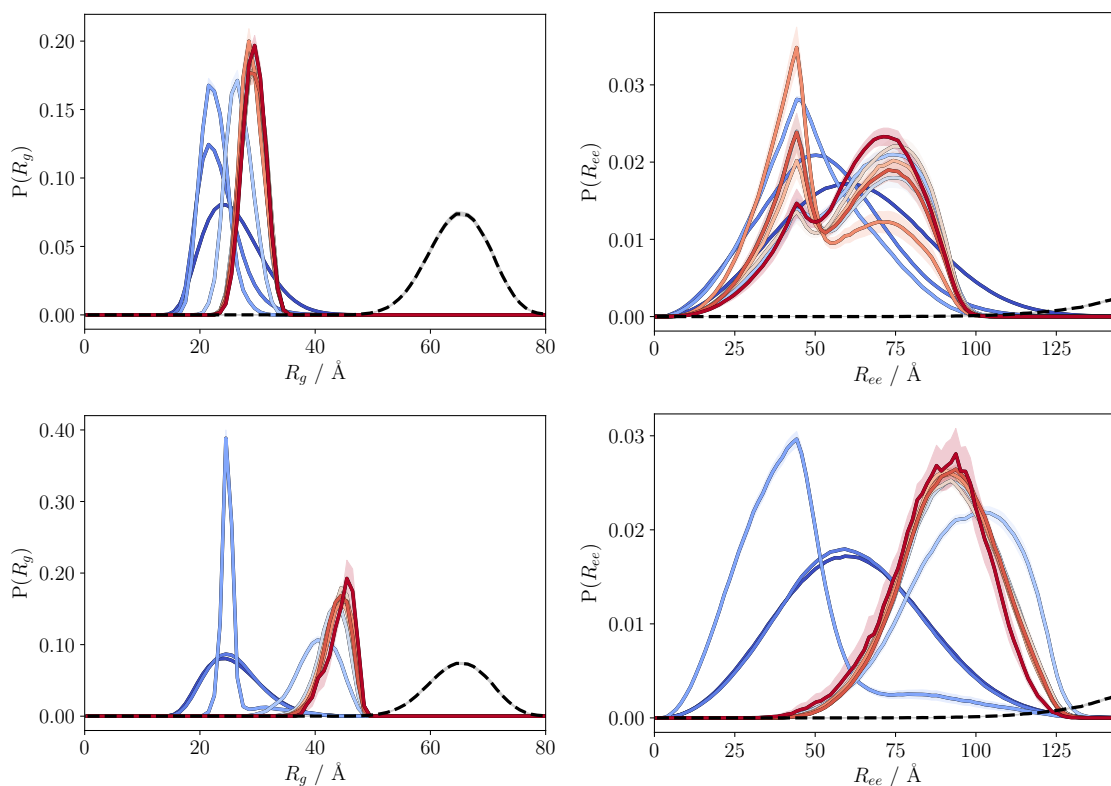

Figure 8: Radius of gyration and end-to-end radius for PE for increasing pH, starting at $pH-pK_0$ = -4 (dark blue) to 5 (dark red). $d = 7$ (top) and 39 Å (bottom). Dashed line shows system with PE only at $pH-pK_0 = 4$ (fully charged), shaded area shows one standard deviation of the sampled mean.

When the PE is only adsorbed to a single NP the distributions are shifted to smaller R_g and R_{ee} with the former also giving very narrow distributions.
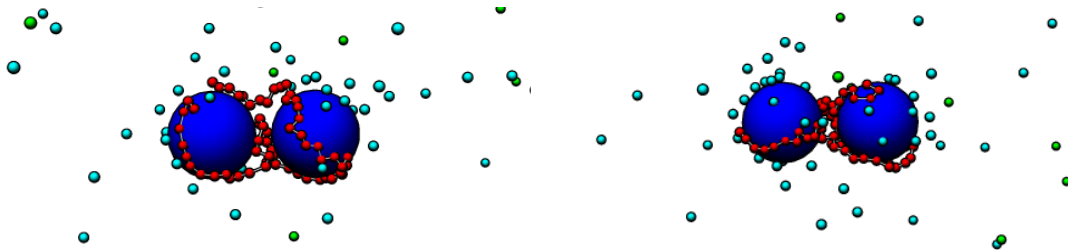
17

Figure 9: Examples of two systems at $d = 7$ Å where the chain ends are situated close together on the same NP (left) and on opposite NPs (right).

Considering pH variations, a free PE will have a large size increase from a compact to an extended state with increasing pH/monomer charge. In comparison, R_g of the PE chain in a system with a single NP which it adsorbs to, is dependent on the NP radius, and – if the PE can overcharge the NP sufficiently and is long enough – the PE length.[41] In the case with two NPs, R_g is affected both by to the PE wrapping around the NPs, and whether it has the space to stretch out between the NPs. At short d, the increase in R_g with pH comes mainly from the intrachain repulsive interactions, as more monomers are charged. This promotes some stretching of the PE and improved wrapping around the NPs, and also leads to the appearance of the bimodal distribution in the R_{ee} distribution, more predominantly for intermediate and high pH values (top panels, Fig. 8).

The bimodal distribution arises, again, due to the PE adsorbing on both NPs in both multi and single link configurations. At short d, the electric field created by the NPs is at its highest close to the center of the system, with a profile similar to the counterion distribution at low pH in Fig. 4. This causes the PE to create multiple links between the NPs, with a larger fraction of the monomers situated close to the center at high pH as seen in Fig. 4, particularly at low pH. This increases the probability of the chain ends being close to each other, giving rise to the peak of R_{ee} around 44 Å, while still allowing for the chain ends to be at opposite ends of the NPs, as evidenced by the peak closer to 75 Å. Both an increase in pH and distance will cause the chain to stretch out more, decreasing the probability of the chain ends being located close to each other. At larger d, the PE will only form a single link between the NPs (as is the case for $d \geq 19$ here), ensuring a minimum distance between the chain ends and giving a unimodal P(R_{ee}). While the end monomers of the PE will sometimes be situated close by each other,

the PE itself will stretch out to cover more of the NPs, as seen in Fig. 9. As such, $P(R_g)$ is unimodal irrespective of pH and NP-NP separation distance, as the chain itself does not switch between a compact and extended configuration.

For larger d, the change in R_g with increasing pH is more pronounced (bottom panels, Fig. 8), due to the increasing bridge length between the NPs. As with the R_g, the end-to-end radius R_{ee} can be seen to increase as PE ionization is increased; at low pH, the PE goes from being free, to adsorbing to a single NP (or occupying the space between the NPs) and presenting a size distribution shifted to smaller values, and finally adsorbing to both NPs, stretching further out.

For simplicity, the system does not contain salt, as low to moderate amounts of electrolyte are not expected to significantly affect the results and conclusions. Salt will in general cause some screening of the electrostatic interactions, which could influence the pH at which the PE becomes charged and the interaction strength between charged particles, which in this case includes the distance at which the PE will form a bridge. The results of shorter simulations with salt at concentrations of 10 mM and 100 mM have been been included in the supplementary information. Here, it is seen that the titration curve is pushed to the right with increasing salt concentration (Fig. S3), as previously seen.[49] Regarding density distributions (Fig. S4), these have a similar shape at concentrations of 10 mM, when compared to the case with no salt. For example, the effect of salt on the bridge formation at $pH-pK_0 = -2$ is not large either, as seen in Fig. S5. High salt concentrations (100 mM) leads to a larger asymmetry, as the transition between the bridging and non-bridging states occurs at shorter NP-NP separations.

Conclusion

We have utilized coarse-grained Monte Carlo simulations to study the interaction between an annealed PE and two charged NPs. This was done for different NP-NP separation distances and increasing pH. In the systems studied, the PE could achieve a total charge equal to a single NP, allowing it to create a neutral complex when adsorbed on a single NP. This occured at the longest separation distances, around 45 Å. Although the PE was adsorbed on a single NP, the

monomers were not uniformly distributed on the surface, as the attraction from the other NP caused a small bias in the density distribution. This was moreso the case at shorter separation distances, where the PE would bridge the nanoparticles, with multiple links at the shortest distances. A similar bias was also observed for the NP counterion density around the NP. The separation distances where bridging between the nanoparticles occured, were dependent on the solution pH and the fractional charge of the PE, with bridging being more likely for higher PE charge/pH. This indicates that annealed PEs can be used to control the aggregation and creation of larger or smaller NP-PE complexes in real systems by changing the pH. This is assuming the concentration of PEs and NPs provide a sufficiently large NP-NP distance and allow for over- or undercharged complexes.

Properties of the system with an annealed PE were also compared to a system with a quenched homopolymer, with charge independent of pH. It was found that for PEs of similar, and small, fractional charge, there was a difference in the PE-NP adsorption behaviour between the annealed and quenched PE. This is attributed to the difference in charge density along the PE chain, with the annealed PE having a stronger adsorption due to the large charge of a few monomers located in close proximity on the PE due to the mobility of the charges, as compared with the evenly distributed and small charge of the quenched PE. Whereas the annealed PE adsorbed on the NPs, creating a link consisting mostly of neutral monomers, the corresponding quenched PE occupied more of the space between the PEs. At higher average ionization of the PE, the difference in adsorption between the annealed and quenched systems is found mainly in the ability to form a bridge between the NPs, with the annealed PE being able to form a bridge at longer NP separation distances.

The results outlined here, could partially elucidate experimental observations, as discussed, and can aid in the design of pH responsive systems where single to multiple NP complexes are desirable such as in controlled NP deposition. The impact of PE charge density and architecture on the adsorption process will be further elucidated in upcoming work.

Supporting information

Supporting information is available, containing more results on annealed and quenched PEs (monomer density distributions for d of 26 – 36 Å and bridging probability as a function of distance), and selected results of systems with salt.

Acknowledgements

References

(1) Evans, D. F.; Wennerström, H. *The Colloidal Domain: Where Physics, Chemistry, Biology and Technology Meet*; Wiley-VCH, 1999.

(2) Butt, H.-J.; Graf, K.; Kappl, M. *Physics and Chemistry of Interfaces*; Wiley-VCH, 2006.

(3) Netz, R. R.; Andelman, D. Neutral and charged polymers at interfaces. *Phys. Rep.* **2003**, *380*, 1 – 95.

(4) Kleshchanok, D.; Tuinier, R.; Lang, P. R. Direct measurements of polymer-induced forces. *J. Phys.: Condens. Matter* **2008**, *20*, 073101.

(5) Linse, P. Interaction between colloids with grafted diblock polyampholytes. *J. Chem. Phys* **2007**, *126*, 114903.

(6) Szilagyi, I.; Trefalt, G.; Tiraferri, A.; Maroni, P.; Borkovec, M. Polyelectrolyte adsorption, interparticle forces, and colloidal aggregation. *Soft Matter* **2014**, *10*, 2479–2502.

(7) Korpi, A.; Ma, C.; Liu, K.; Nonappa,; Herrmann, A.; Ikkala, O.; Kostiainen, M. A. Self-assembly of electrostatic cocrystals from supercharged fusion peptides and protein cages. *ACS Macro Lett.* **2018**, *7*, 318–323.

(8) Podgornik, R. Two-body polyelectrolyte-mediated bridging interactions. *J. Chem. Phys* **2003**, *118*, 11286–11296.

(9) Podgornik, R.; Ličer, M. Polyelectrolyte bridging interactions between charged macromolecules. *Curr. Opin. Colloid Interface Sci.* **2006**, *11*, 273–279.

(10) de Vries, R.; Stuart, M. C. Theory and simulations of macroion complexation. *Curr. Opin. Colloid Interface Sci.* **2006**, *11*, 295–301.

(11) Forsman, J. Polyelectrolyte mediated forces between macromolecules. *Curr. Opin. Colloid Interface Sci.* **2006**, *11*, 290–294.

(12) Tong, C.; Zhu, Y.; Zhang, H.; Qiu, F.; Tang, P.; Yang, Y. The self-consistent field study of the adsorption of flexible polyelectrolytes onto two charged nano-objects. *J. Phys. Chem. B* **2011**, *115*, 11307–11317.

(13) Tong, C. The interplay of the polyelectrolyte-surface electrostatic and non-electrostatic interactions in the polyelectrolytes adsorption onto two charged objects âĂŞ A selfconsistent field study. *J. Chem. Phys* **2012**, *137*, 104904.

(14) Forsman, J.; Nordholm, S. Polyelectrolyte mediated interactions in colloidal dispersions: Hierarchical screening, simulations, and a new classical density functional theory. *Langmuir* **2012**, *28*, 4069–4079.

(15) Forsman, J. Surface forces in electrolytes containing polyions and oppositely charged surfaces. *Curr. Opin. Colloid Interface Sci.* **2017**, *27*, 57–62.

(16) Podgornik, R.; Åkesson, T.; Jönsson, B. Colloidal interactions mediated via polyelectrolytes. *J. Chem. Phys* **1995**, *102*, 9423–9434.

(17) Ličer, M.; Podgornik, R. Polyelectrolyte-mediated bridging interactions: columnar macromolecular phases. *J. Phys.: Condens. Matter* **2010**, *22*, 414102.

(18) Turesson, M.; Forsman, J.; Åkesson, T. Surface forces mediated by charged polymers: effects of intrinsic chain stiffness. *Langmuir* **2006**, *22*, 5734–5741.

(19) Truzzolillo, D.; Bordi, F.; Sciortino, F.; Sennato, S. Interaction between like-charged polyelectrolyte-colloid complexes in electrolyte solutions: A Monte Carlo simulation study in the Debye-Hückel approximation. *J. Chem. Phys* **2010**, *133*, 024901.

(20) Ulrich, S.; Seijo, M.; Laguecir, A.; Stoll, S. Nanoparticle adsorption on a weak polyelectrolyte. Stiffness, pH, charge mobility, and ionic concentration effects investigated by Monte Carlo simulations. *J. Phys. Chem. B* **2006**, *110*, 20954–20964.

(21) Poptoshev, E.; Rutland, M. W.; Claesson, P. M. Surface Forces in Aqueous Polyvinylamine Solutions. I. Glass Surfaces. *Langmuir* **1999**, *15*, 7789–7794.

(22) Maurdev, G.; Meagher, L.; Ennis, J.; Gee, M. L. Surface forces between adsorbed quaternarized poly(2-vinylpyridine) layers: Molecular rearrangements and bridging interactions. *Macromolecules* **2001**, 4151–4158.

(23) Zhou, Y.; Gan, Y.; Wanless, E. J.; Jameson, G. J.; Franks, G. V. Interaction forces between silica surfaces in aqueous solutions of cationic polymeric flocculants: Effect of polymer charge. *Langmuir* **2008**, *24*, 10920–10928.

(24) Böhmer, M. R.; Evers, O. A.; Scheutjens, J. M. H. M. Weak polyelectrolytes between two surfaces: Adsorption and stabilization. *Macromolecules* **1990**, *23*, 2288–2301.

(25) Claesson, P. M.; Poptoshev, E.; Blomberg, E.; Dedinaite, A. Polyelectrolyte-mediated surface interactions. *Adv. Colloid Interface Sci.* **2005**, *114-115*, 173–187.

(26) Borkovec, M.; Papastavrou, G. Interactions between solid surfaces with adsorbed polyelectrolytes of opposite charge. *Curr. Opin. Colloid Interface Sci.* **2008**, *13*, 429–437.

(27) Borkovec, M.; Szilagyi, I.; Popa, I.; Finessi, M.; Sinha, P.; Maroni, P.; Papastavrou, G. Investigating forces between charged particles in the presence of oppositely charged polyelectrolytes with the multi-particle colloidal probe technique. *Adv. Colloid Interface Sci.* **2012**, *179-182*, 85–98.

(28) Berret, J.-F.; Cristobal, G.; Hervé, P.; Oberdisse, J.; Grillo, I. Structure of colloidal complexes obtained from neutral/poly- electrolyte copolymers and oppositely charged surfactants. *Eur. Phys. J. E* **2002**, *9*, 301–311.

(29) Drogoz, A.; David, L.; Rochas, C.; Domard, A.; Delair, T. Polyelectrolyte complexes from polysaccharides: Formation and stoichiometry monitoring. *Langmuir* **2007**, *23*, 10950–10958.

(30) van der Gucht, J.; Spruijt, E.; Lemmers, M.; Stuart, M. A. C. Polyelectrolyte complexes: Bulk phases and colloidal systems. *J. Colloid Interface Sci.* **2011**, *361*, 407–422.

(31) Norrman, J.; Lynch, I.; Piculell, L. Phase behavior of aqueous polyion-surfactant ion complex salts: Effects of polyion charge density. *J. Phys. Chem. B* **2007**, *111*, 8402–8410.

(32) Carnal, F.; Ulrich, S.; Stoll, S. Influence of explicit ions on titration curves and conformations of flexible polyelectrolytes: A Monte Carlo study. *Macromolecules* **2010**, *43*, 2544–2553.

(33) Carnal, F.; Stoll, S. Adsorption of weak polyelectrolytes on charged nanoparticles. Impact of salt valency, pH, and nanoparticle charge density. Monte Carlo simulations. *J. Phys. Chem. B* **2011**, *115*, 12007–12018.

(34) Ulrich, S.; Seijo, M.; Carnal, F.; Stoll, S. Formation of complexes between nanoparticles and weak polyampholyte chains. Monte Carlo simulations. *Macromolecules* **2011**, *44*, 1661–1670.

(35) Carnal, F.; Clavier, A.; Stoll, S. Polypeptide-nanoparticle interactions and corona formation Investigated by Monte Carlo simulations. *Polymers* **2016**, *8*, 203.

(36) de Oliveira, V. M.; de Carvalho, S. J. Adsorption of pH-responsive polyelectrolyte chains onto spherical macroions. *Eur. Phys. J. E* **2014**, *37*, 75.

(37) Reed, C. E.; Reed, W. F. Monte Carlo study of titration of linear polyelectrolytes. *J. Chem. Phys* **1992**, *96*, 1609–1620.

(38) Ullner, M. In *Handbook of Polyelectrolytes and Their Applications*; Tripathy, S. K., Kumar, J., Nalwa, H. S., Eds.; American Scientific Publishers, 2002; Vol. 3; Chapter 10, pp 271–308.

(39) Reščič, J.; Linse, P. MOLSIM: A modular molecular simulation software. *J. Comput. Chem.* **2015**, *36*, 1259–1274.

(40) Ullner, M.; Jönsson, B.; Söderberg, B.; Peterson, C. A Monte Carlo study of titrating polyelectrolytes. *J. Chem. Phys* **1996**, *104*, 3048–3057.

(41) Stornes, M.; Linse, P.; Dias, R. S. Monte Carlo simulations of complexation between weak polyelectrolytes and a charged nanoparticle. Influence of polyelectrolyte chain length and concentration. *Macromolecules* **2017**, *50*, 5978–5988.

(42) Uhlík, F.; Košovan, P.; Limpouchová, Z.; Procházka, K.; Borisov, O. V.; Leermakers, F. A. M. Modeling of ionization and conformations of starlike weak polyelectrolytes. *Macromolecules* **2014**, *47*, 4004–4016.

(43) Hofzumahaus, C.; Hebbeker, P.; Schneider, S. Monte Carlo simulations of weak polyelectrolyte microgels: pH-dependence of conformation and ionization. *Soft Matter* **2018**, *14*, 4087 – 4100.

(44) van Opheusden, J. H. J. Polyelectrolytes between two membranes or colloidal particles. *J. Phys. A: Math. Gen.* **1988**, *21*, 2739.

(45) Forsman, J. Polyelectrolyte adsorption: Electrostatic mechanisms and nonmonotonic responses to salt addition. *Langmuir* **2012**, *28*, 5138–5150.

(46) Liu, H.; Huang, S.; Li, X.; Zhang, L.; Tan, Y.; Wei, C.; Lv, J. Facile fabrication of novel polyhedral oligomeric silsesquioxane/carboxymethyl cellulose hybrid hydrogel based on supermolecular interactions. *Mater. Lett.* **2013**, *90*, 142–144.

(47) Yoshida, K.; Dubin, P. L. Complex formation between polyacrylic acid and cationic/nonionic mixed micelles: effect of pH on electrostatic interaction and hydro-

gen bonding. *Colloids and Surfaces A: Physicochemical and Engineering Aspects* **1999**, *147*, 161 – 167.

(48) Cooper, C. L.; Goulding, A.; Kayitmazer, A. B.; Ulrich, S.; Stoll, S.; Turksen, S.; ichi Yusa, S.; Kumar, A.; Dubin, P. L. Effects of polyelectrolyte chain stiffness, charge mobility, and charge sequences on binding to proteins and micelles. *Biomacromolecules* **2006**, *7*, 1025–1035.

(49) Ulrich, S.; Laguecir, A.; Stoll, S. Complex formation between a nanoparticle and a weak polyelectrolyte chain: Monte Carlo simulations. *J. Nanoparticle Res.* **2004**, *6*, 595–603.

Graphical TOC Entry